References

1. Hashimoto K, Ishiwata K. Sigma receptor ligands: possible application as therapeutic drugs and as radiopharmaceuticals. Curr Pharm Des 2006;12:3857–76.
2. Walker JM, Bowen WD, Walker FO, Matsumoto RR, De Costa B, Rice KC. Sigma receptors: biology and function. Pharmacol Rev 1990;42:355–402.
3. Quirion R, Bowen WD, Itzhak Y, Junien JL, Musacchio JM, Rothman RB, et al. A proposal for the classification of sigma binding sites. Trends Pharmacol Sci 1992;13:85–6.
4. Su TP, London ED, Jaffe JH. Steroid binding at sigma receptors suggests a link between endocrine, nervous, and immune systems. Science (New York) 1988;240:219–21.
5. Su TP. Delineating biochemical and functional properties of sigma receptors: emerging concepts. Critical Rev Neurobiol 1993;7:187–203.
6. Bowen WD. Sigma receptors: recent advances and new clinical potentials. Pharm Acta Helv 2000;7:211–8.
7. Maurice T, Urani A, Phan VL, Romieu P. The interaction between neuroactive steroids and the sigma$_1$ receptor function: behavioral consequences and therapeutic opportunities. Brain Res Rev 2001;37:116–32.
8. Hiramatsu M, Hoshino T, Kameyama T, Nabeshima T. Involvement of kappa-opioid and sigma receptors in short-term memory in mice. Eur J Pharmacol 2002;453:91–8.
9. Maurice T, Hiramatsu M, Kameyama T, Hasegawa T, Nabeshima T. Behavioral evidence for a modulating role of sigma ligands in memory processes. II. Reversion of carbon monoxide-induced amnesia. Brain Res 1994;647:57–64.
10. Senda T, Matsuno K, Okamoto K, Kobayashi T, Nakata K, Mita S. Ameliorating effect of SA4503, a novel sigma$_1$ receptor agonist, on memory impairments induced by cholinergic dysfunction in rats. Eur J Pharmacol 1996;315:1–10.
11. Matsuno K, Matsunaga K, Senda T, Mita S. Increase in extracellular acetylcholine level by sigma ligands in rat frontal cortex. J Pharmacol Exp Ther 1993;265:851–9.
12. Matsuno K, Senda T, Kobayashi T, Mita S. Involvement of sigma$_1$ receptor in (+)-N-allylnormetazocine-stimulated hippocampal cholinergic functions in rats. Brain Res 1995;690:200–6.
13. Kobayashi T, Matsuno K, Nakata K, Mita S. Enhancement of acetylcholine release by SA4503, a novel sigma$_1$ receptor agonist, in the rat brain. J Pharmacol Exp Ther 1996;279:106–13.
14. Ishiwata K, Kobayashi T, Kawamura K, Matsuno K. Age-related changes of the binding of [^{3}H]SA4503 to sigma$_1$ receptors in the rat brain. Ann Nucl Med 2003;17:73–7.
15. Kawamura K, Kimura Y, Tsukada H, Kobayashi T, Nishiyama S, Kakiuchi T, et al. An increase of sigma receptors in the aged monkey brain. Neurobiol Aging 2003;24:745–52.
16. Weissman AD, Casanova MF, Kleinman JE, London ED, De Souza EB. Selective loss of cerebral cortical sigma, but not PCP binding sites in schizophrenia. Biol Psychiatry 1991;29:41–54.
17. Matsuno K, Kobayashi T, Tanaka MK, Mita S. Sigma$_1$ receptor subtype is involved in the relief of behavioral despair in the mouse forced swimming test. Eur J Pharmacol 1996;312:267–71.
18. Lobner D, Lipton P. Sigma-ligands and non-competitive NMDA antagonists inhibit glutamate release during cerebral ischemia. Neurosci Lett 1990;117:169–74.
19. Mishina M, Ishiwata K, Ishii K, Kitamura S, Kimura Y, Kawamura K, et al. Function of sigma receptors in Parkinson's disease. Acta Neurol Scand 2005;112:103–7.
20. Jansen KL, Faull RL, Storey P, Leslie RA. Loss of sigma binding sites in the CA1 area of the anterior hippocampus in Alzheimer's disease correlates with CA1 pyramidal cell loss. Brain Res 1993;623:299–302.
21. Maurice T. Improving Alzheimer's disease-related cognitive deficits with sigma$_1$ receptor agonists. Drug News Perspect 2002;15:617–25.
22. Ishiwata K, Tsukada H, Kawamura K, Kimura Y, Nishiyama S, Kobayashi T, et al. Mapping of CNS sigma$_1$ receptors in the conscious monkey: preliminary PET study with [^{11}C]SA4503. Synapse 2001;40:235–7.
23. Kawamura K, Ishiwata K, Tajima H, Ishii S, Matsuno K, Homma Y, et al. In vivo evaluation of [^{11}C]SA4503 as a PET ligand for mapping CNS sigma$_1$ receptors. Nucl Med Biol 2000;27:255–61.
24. Sakata M, Kimura Y, Naganawa M, Oda K, Ishii K, Chihara K, et al. Mapping of human cerebral sigma$_1$ receptors using positron emission tomography and [^{11}C]SA4503. Neuroimage 2007;35:1–8.
25. McKhann G, Drachman D, Folstein M, Katzman R, Price D, Stadlan EM. Clinical diagnosis of Alzheimer's disease: report of the NINCDS-ADRDA Work Group under the auspices of Department of Health and Human Services Task Force on Alzheimer's Disease. Neurology 1984;34:939–44.
26. Herholz K, Salmon E, Perani D, Baron JC, Holthoff V, Frolich L, et al. Discrimination between Alzheimer dementia and controls by automated analysis of multicenter FDG PET. Neuroimage 2002;17:302–16.
27. Minoshima S, Giordani B, Berent S, Frey KA, Foster NL, Kuhl DE. Metabolic reduction in the posterior cingulate cortex in very early Alzheimer's disease. Ann Neurol 1997;42:85–94.
28. Reisberg B, Borenstein J, Salob SP, Ferris SH, Franssen E, Georgotas A. Behavioral symptoms in Alzheimer's disease: phenomenology and treatment. J Clin Psychiatry 1987;48 Suppl:9–15.
29. Folstein MF, Folstein SE, McHugh PR. "Mini-Mental State". A practical method for grading the cognitive state of patients for the clinician. J Psychiatr Res 1975;12:189–98.
30. Hughes CP, Berg L, Danziger WL, Coben LA, Martin RL. A new clinical scale for the staging of dementia. Br J Psychiatry 1982;140:566–72.
31. Fujiwara T, Watanuki S, Yamamoto S, Miyake M, Seo S, Itoh M, et al. Performance evaluation of a large axial field-of-view PET scanner: SET-2400 W. Ann Nucl Med 1997;11:307–13.
32. Mishina M, Senda M, Kimura Y, Toyama H, Ishiwata K, Ohyama M, et al. Intrasubject correlation between static scan and distribution volume images for [^{11}C]flumazenil PET. Ann Nucl Med 2000;14:193–8.
33. Logan J. A review of graphical methods for tracer studies and strategies to reduce bias. Nucl Med Biol 2003;30:833–44.
34. Mielke R, Schroder R, Fink GR, Kessler J, Herholz K, Heiss WD. Regional cerebral glucose metabolism and postmortem pathology in Alzheimer's disease. Acta Neuropathol (Berl) 1996;91:174–9.
35. Ohyama M, Senda M, Ishiwata K, Kitamura S, Mishina M, Ishii K, et al. Preserved benzodiazepine receptors in Alzheimer's disease measured with C-11 flumazenil PET and I-123 iomazenil SPECT in comparison with CBF. Ann Nucl Med 1999;13:309–15.
36. Nordberg A. PET imaging of amyloid in Alzheimer's disease. Lancet Neurol 2004;3:519–27.
37. Braak H, Braak E, Bohl J, Lang W. Alzheimer's disease: amyloid plaques in the cerebellum. J Neurol sci 1989;93:277–87.

38. Ishii K, Sasaki M, Kitagaki H, Yamaji S, Sakamoto S, Matsuda K, et al. Reduction of cerebellar glucose metabolism in advanced Alzheimer's disease. J Nucl Med 1997;38:925–8.
39. Larner AJ. The cerebellum in Alzheimer's disease. Dement Geriatr Cogn Disord 1997;8:203–9.
40. Wegiel J, Wisniewski HM, Dziewiatkowski J, Badmajew E, Tarnawski M, Reisberg B, et al. Cerebellar atrophy in Alzheimer's disease-clinicopathological correlations. Brain Res 1999;818:41–50.
41. Sjöbeck M, Englund E. Alzheimer's disease and the cerebellum: a morphologic study on neuronal and glial changes. Dement Geriatr Cogn Disord 2001;12:211–8.
42. Verdile G, Gnjec A, Miklossy J, Fonte J, Veurink G, Bates K, et al. Protein markers for Alzheimer disease in the frontal cortex and cerebellum. Neurology 2004;63:1385–92.
43. Sultana R, Boyd-Kimball D, Poon HF, Cai J, Pierce WM, Klein JB, et al. Redox proteomics identification of oxidized proteins in Alzheimer's disease hippocampus and cerebellum: an approach to understand pathological and biochemical alterations in AD. Neurobiol Aging 2006;27:1564–76.
44. Chaki S, Okuyama S, Ogawa S, Tomisawa K. Regulation of NMDA-induced [^{3}H]dopamine release from rat hippocampal slices through sigma-1 binding sites. Neurochem Int 1998;33:29–34.

Ann Nucl Med (2008) 22:841–847
DOI 10.1007/s12149-008-0185-5

ORIGINAL ARTICLE

Adenosine A_1 receptors using 8-dicyclopropylmethyl-1-[^{11}C]methyl-3-propylxanthine PET in Alzheimer's disease

**Nobuyoshi Fukumitsu · Kenji Ishii · Yuichi Kimura
Keiichi Oda · Masaya Hashimoto · Masahiko Suzuki
Kiichi Ishiwata**

Received: 5 September 2007 / Accepted: 19 June 2008

Abstract
Objective Adenosine is an endogenous modulator of synaptic functions in the central nervous system. The effects of adenosine are mediated by at least four adenosine receptor subtypes. Decreased density of adenosine A_1 receptors, which is a major subtype adenosine receptor in the hippocampus, has been reported in vitro in Alzheimer's disease. We evaluated adenosine A_1 receptor in the brain of elderly normal subjects and patients with Alzheimer's disease (n = 8 and 6, respectively), using positron emission tomography (PET) and 8-dicyclopropylmethyl-1-[^{11}C]methyl-3-propylxanthine ([^{11}C]MPDX).
Methods A 60-min PET scan with [^{11}C]MPDX was performed. The patients with Alzheimer's disease also underwent PET with [^{18}F]fluorodeoxyglucose (FDG). The binding potential of [^{11}C]MPDX was quantitatively calculated in the regions of interest (ROIs) placed on the frontal, medial frontal, temporal, medial temporal, parietal, and occipital cortices, striatum, thalamus, cerebellum, and pons. Statistical parametric mapping (SPM2) was used for analysis of [^{11}C]MPDX and FDG-PET.
Results In the ROI-based analysis, the binding potential of [^{11}C]MPDX in patients with Alzheimer's disease was significantly lower in the temporal and medial temporal cortices and thalamus than that in elderly normal subjects (P = 0.038, 0.028, and 0.039, respectively). SPM analysis also showed significant decreased binding potential in the temporal and medial temporal cortices and thalamus in patients with Alzheimer's disease. FDG uptake was significantly decreased in the temporoparietal cortex and posterior cingulate gyrus.
Conclusions Decreased binding of [^{11}C]MPDX in patients with Alzheimer's disease was detected in temporal and medial temporal cortices and thalamus. This pattern possibly differed from the hypometabolism pattern of FDG. [^{11}C]MPDX PET is valuable for the detection of degeneration in the temporal and medial temporal cortices and corticothalamic transmission, and may provide a different diagnostic tool from FDG-PET in brain disorders such as Alzheimer's disease.

Keywords [^{11}C]MPDX · Adenosine A_1 receptor · Medial temporal cortex · Positron emission tomography · Alzheimer's disease

N. Fukumitsu (✉)
2-1-1-204 Midoridai, Funabashi, Chiba 274-0818, Japan
e-mail: fukumitsun@yahoo.co.jp

N. Fukumitsu
Proton Medical Research Center, University of Tsukuba, Ibaraki, Japan

N. Fukumitsu · K. Ishii · Y. Kimura · K. Oda · K. Ishiwata
Positron Medical Center, Tokyo Metropolitan Institute of Gerontology, Tokyo, Japan

M. Hashimoto · M. Suzuki
Department of Neurology, Jikei University School of Medicine, Tokyo, Japan

Introduction

Adenosine is present in large amounts in the mammalian brain and plays a role as an endogenous modulator of synaptic functions in the central nervous system. Prior work has established a role for adenosine in a diverse array of neural phenomena, which include regulation of

sleep and the level of arousal, neuroprotection, regulation of seizure susceptibility, locomotor effects, analgesia, mediation of the effects of ethanol, and chronic drug use [1]. Therefore, interaction with the adenosine metabolism is a promising target for therapeutic intervention in ischemic, neurological, and psychiatric disorders [2–4].

The effects of adenosine are mediated by at least four adenosine receptor subtypes, namely, A_1, A_{2A}, A_{2B}, and A_3. The two major subtypes of receptors, namely, A_1 and A_2 receptors, have been well investigated in molecular biology, pharmacology, and physiology [4–6]. Adenosine presynaptically inhibits the release of many neurotransmitters, especially excitatory ones such as the potentially excitotoxic amino acid glutamate [7, 8]. This effect of adenosine is mediated by presynaptic A_1 receptors linked via G-proteins to both calcium and potassium ion channels [9–12].

Alzheimer's disease is the most common form of age-related dementia and one of the most serious health problems. Dementia affects approximately 1–5% of the population more than 65 years of age [13] and 20–40% of the population more than 80 years of age [14, 15]. The economic and social burdens of Alzheimer's disease on families have been documented in many studies [16–18]. In studies on the postmortem brain with Alzheimer's disease, decreased density of adenosine A_1 receptor in the hippocampus has been reported [19–22]. Ulas et al. [20] reported that the reduction in the adenosine A_1-specific ligand-receptor binding was owing to a decrease in the density of binding sites (B_{max}), but was not owing to changes in the affinity (K_d) [20]. With regard to the clinical diagnosis of Alzheimer's disease, positron emission tomography (PET) using [^{18}F]fluorodeoxyglucose (FDG) is the most popular method, and reduction of glucose metabolism is prominent in the temporo-parietal cortex and posterior cingulate gyrus. However, hypometabolism in the medial temporal cortex has not necessarily been detected as a symptom of Alzheimer's disease, although morphological changes are prominent in the medial temporal cortex [23–25].

Recently, we successfully performed imaging of adenosine A_1 receptors in the human brain of normal young volunteers using PET with 8-dicyclopropylmethyl-1-[^{11}C]methyl-3-propylxanthine ([^{11}C]MPDX) [26–29]. In the present study, we investigated the change of the adenosine A_1 receptors in patients with Alzheimer's disease with [^{11}C]MPDX PET. We also examined the same patients with FDG-PET for direct comparison of the two diagnostic tools. This report is a preliminary study of the utility of [^{11}C]MPDX PET in the diagnosis of patients with Alzheimer's disease.

Materials and methods

The study protocol was approved by the Institutional Ethical Committee. Eight normal elderly volunteers [men 66.9 ± 6.5 (61–75) years] were enrolled together with six Alzheimer's disease patients [men, $n = 5$; women, $n = 1$; 73.5 ± 9.8 (58–83) years]. A written informed consent was obtained from all the participants in this study. It was confirmed that no participants received xanthine-type drugs such as theophylline for asthma.

All the normal subjects were healthy according to the history, physical, neurological and psychiatric examinations, and a magnetic resonance imaging (MRI) study of the brain prior to the PET study. In the psychiatric examination, we used the Hospital Anxiety and Depression Scale [30].

All the patients with Alzheimer's disease showed mild-to-moderate dementia and were diagnosed according to the National Institute of Neurological and Communicative Diseases and Stroke/Alzheimer's Disease and Related Disorders Association (NINCDS–ADRDA) criteria. The disease duration following the first onset of memory disturbance was 0–4 years. We performed clinical assessments, including neuropsychological testing and exclusion of other diseases, with computed tomography or MRI as required by the NINCDS–ADRDA criteria. The exclusion criteria were prior episodes of subarachnoid or intracerebral hemorrhage, intracranial tumors, hydrocephalus, all psychoses (including major depression), alcoholism, epilepsy, ischemic strokes, vascular dementia, sleep disorders, and other forms of dementia, anemia, and nonstabilized diabetes mellitus. The patients who were suspected to have other diseases with neurodegeneration from the FDG-PET findings or who were on medications that affect the brain circulation or metabolism were excluded, and especially acethylcholinesterase blockers were not given prior to the PET study. The Mini-Mental State Examination score was 20–24. Neither normal subjects nor patients with Alzheimer's disease complained about their sleep behavior.

PET measurement

Radiosynthesis of [^{11}C]MPDX was performed as described earlier [31, 32]. PET measurement was performed with an SET-2400W system (Shimadzu, Kyoto, Japan), which acquires 63 slices having 128 × 128 pixels each at a transverse resolution of 4.5 mm full width at half maximum (FWHM) and at an axial resolution of 5.8 mm FWHM. Scanning took place as the subjects lay supine. A venous catheter was inserted into the forearm vein of the subjects for tracer injection, and an arterial

catheter was inserted into the distal radial artery under local anesthesia for arterial blood sampling. After positioning the subject's head in the canthomeatal orientation and fixing the subject's head using a band to prevent movement during the examination, a transmission scan was performed with a rotating [^{68}Ga]/[^{68}Ge] line source to correct for the photon attenuation using the attenuation map. All the subjects were given [^{11}C]MPDX [611 ± 123 (300–757) MBq/14.4 ± 12.5 (2.8–47.5 nmol)] for a period of 10 s, and the PET scan and arterial blood sampling were performed for 60 min as described earlier [27]. We did not impose any meal restriction for [^{11}C]MPDX PET.

In all patients with Alzheimer's disease, FDG-PET was also done on the same day or within 3 months. The subjects each received an intravenous injection of FDG [128 ± 13 (107–142) MBq]. Starting 45 min post-injection, an emission scan was performed for 6 min following a transmission scan using ^{68}Ge for attenuation correction. In the case of one of the six patients who underwent both [^{11}C]MPDX PET and FDG-PET on the same day, the former was carried out in the morning, with FDG administered 3 h later.

Kinetic analysis

The PET images were registered and resliced to the MRI with Ardekani's-image registration algorithm [33] using UNIX workstations (Silicon Graphics, Mountain View, CA, USA) with the Dr. View image analysis software system (AJS, Tokyo, Japan). Regions of interest (ROIs) were placed on the frontal, medial frontal, temporal, medial temporal, parietal, and occipital cortices, striatum, thalamus, cerebellum, and pons based on MRI (Fig. 1). The ROI on the frontal cortex had 1582 ± 275 voxels and that on the pons had 85 ± 3 voxels (1 voxel = 2 mm × 2 mm × 6.25 mm). The voxel numbers on other regions were in-between these values. Using the time–activity curves for each ROI of the brain and the metabolite-corrected time–activity curve of plasma, the distribution volume (DV) of [^{11}C]MPDX in each ROI was calculated by graphical analysis using Logan plots according to the method as described earlier [27, 28]. The binding potential in each ROI was then obtained as follows [28]:

$$\text{Binding potential} = DV_{(\text{region})}/DV_{(\text{cerebellum})} - 1.$$

The binding potential in each ROI was expressed as mean values ± standard deviations. The difference of the binding potential in each ROI was respectively tested between normal elderly subjects group and patients with Alzheimer's disease group using Mann–Whitney U test.

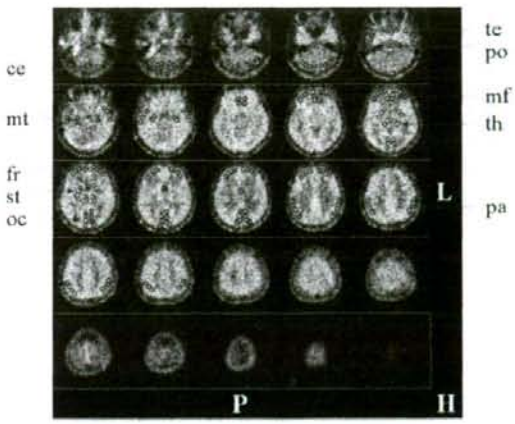

Fig. 1 Region of interest mapping of 8-dicyclopropylmethyl-1-[^{11}C]methyl-3-propylxanthine positron emission tomography ([^{11}C]MPDX PET). *fr* frontal cortex, *mf* medial frontal cortex, *te* temporal cortex, *mt* medial temporal cortex, *pa* parietal cortex, *oc* occipital cortex, *st* striatum, *th* thalamus, *ce* cerebellum, *po* pons

Statistical significance was assumed at $P < 0.05$. In FDG-PET, regional glucose metabolism was expressed using standardized uptake value (SUV).

Statistical parametric mapping analysis

The PET images were analyzed using SPM2 software (Wellcome Department of Cognitive Neurology, Institute of Neurology, London, UK), implemented using Matlab 7.0 (MathWorks, Sherborn, MA, USA). For this purpose, binding potential image of [^{11}C]MPDX and SUV image of FDG were used. Prior to statistical analysis, all the images were spatially normalized into the MNI standard space (Montreal Neurological Institute, McGill University, Montreal, QC, Canada) using house-made templates for [^{11}C]MPDX and FDG-PET images, to remove inter-subject anatomical variability. In normalization of [^{11}C]MPDX PET, total DV image that well reflected brain anatomical structure including cerebellum was used. Spatially normalized images were smoothed by convolution, using an isotropic Gaussian kernel with 16 mm FWHM. The aim of smoothing was to increase the signal-to-noise ratio and to account for the subtle variations in anatomical structures. The count of each voxel in FDG-PET was normalized to the global mean (value = 50) with proportional scaling in SPM2. No global normalization was applied to the [^{11}C]MPDX PET because binding potential was quantitatively calculated. After spatial and count normalization, statistical comparisons between groups were performed on a voxel-by-voxel basis using t statistics, generating SPM (t)

maps. In FDG-PET, the data of the normal elderly template in our institute ($n = 41$, 51–78 years) were used as a reference for the patients with Alzheimer's disease. The data of the normal volunteers whose age and eligibility were matched with this protocol were used in normal elderly template. Thresholds of $P < 0.005$ and $P < 0.01$ corrected for the cluster level were applied to [^{11}C]MPDX and FDG-PET images, respectively. The clusters with an extent of greater than 300 voxels were considered. For visualization of the t score statistics [SPM (t) map], the significant voxels were projected onto the 3D rendered brain of a standard high-resolution MRI template provided by SPM2, thus allowing anatomical identification.

Results

In the ROI-based analysis, the binding potential of [^{11}C]MPDX in normal elderly subjects was high in the striatum and thalamus and low in the cerebellum and pons. The binding potential of [^{11}C]MPDX in patients with Alzheimer's disease was high in the striatum and thalamus and low in the medial temporal cortex and cerebellum. The binding potential of [^{11}C]MPDX in patients with Alzheimer's disease was significantly lower in the temporal, medial temporal cortices, and thalamus than that in normal elderly subjects ($P = 0.038$, 0.028, and 0.039, respectively; Fig. 2). Especially, the binding potential of [^{11}C]MPDX in the medial temporal cortex in patients with Alzheimer's disease was nearly equal to that in the cerebellum.

The SPM analysis of [^{11}C]MPDX PET between patients with Alzheimer's disease and normal elderly subjects is shown in Fig. 3a. The binding potential was widely and severely decreased in the temporal, medial temporal cortices, and thalamus, and partially decreased in the parietal cortex in patients with Alzheimer's disease with significance ($P < 0.005$, corrected $k > 300$). Decreased binding potential was slightly prominent in the left hemisphere.

The SPM analysis of FDG-PET in the same patients with Alzheimer's disease is shown in Fig. 3b. The FDG uptake was widely and severely decreased in the temporoparietal cortex and posterior cingulate gyrus with significance ($P < 0.01$, corrected $k > 300$). Decreased FDG uptake was slightly prominent in the left hemisphere.

Discussion

In Alzheimer's disease subjects, ROI-based analysis and SPM analysis clearly demonstrated the decreased binding potential of [^{11}C]MPDX in the temporal and medial temporal cortices and thalamus when compared with normal elderly subjects as shown in Figs. 2 and 3a. The finding of decreased binding potential in the medial temporal cortex is consistent with past postmortem autoradiographic and pathological studies of patients with Alzheimer's disease [19–22]. Ulas et al. [20] reported that decreased A_1 agonist binding was observed in the CA1 stratum oriens and outer layers of the parahippocampal gyrus, whereas decreased antagonist binding was found in the subiculum and CA3 region. Adenosine A_1 recep-

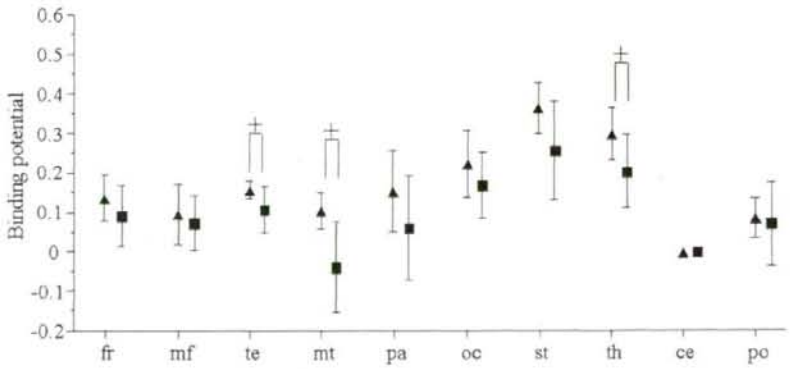

Fig. 2 Binding potential of [^{11}C]MPDX in the human brain. Patients with Alzheimer's disease showed a significantly lower value in the temporal and medial temporal cortices and thalamus than normal elderly volunteers. The value in the cerebellum was zero because the value was calculated based on the assumption that adenosine A_1 receptors are very sparse in the cerebellum. Abbreviations used are the same as in Fig. 1. *Triangle* normal elderly subjects ($n = 8$), *square* patients with Alzheimer's disease ($n = 6$), *plus* $P < 0.05$ compared between normal elderly subjects and patients with Alzheimer's disease

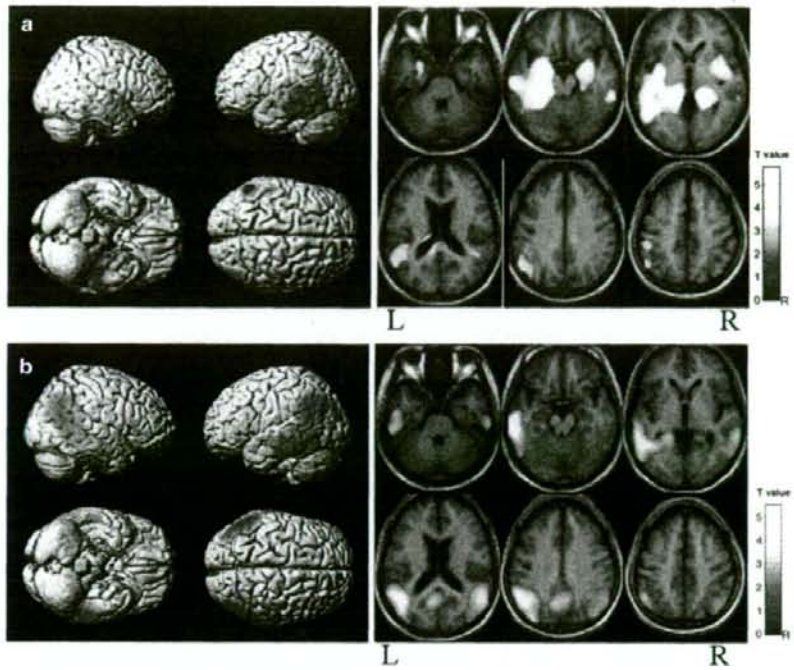

Fig. 3 Statistical analyses of the binding potential of [^{11}C]MPDX (**a**) and standardized uptake value (SUV) of [^{18}F]fluorodeoxyglucose (FDG, **b**) in patients with Alzheimer's disease. *Left* Statistical parametric mapping (SPM) *Z* maps are superimposed onto the right lateral, left lateral, inferior, and superior views (from *left upper* to *right lower*) of a volume-rendered spatially normalized magnetic resonance imaging (MRI) study. *Right* SPM *Z* maps are superimposed onto the axial views of a spatially normalized T1-MRI study. Each image represents from the *bottom* (*left upper*) to the *top* (*right lower*). *Red* and *yellow* represent the areas with significant reduction in binding potential or SUV. **a** Decreased binding potential of [^{11}C]MPDX was noted in the temporal, medial temporal cortices, and thalamus widely and parietal cortex partially. Decreased binding is slightly prominent in the left hemisphere. **b** Decreased SUV of FDG was noted in the temporo-parietal cortices. Decreased SUV is slightly prominent in the left hemisphere

tors are located on the terminal of the perforant pathway which provides a major input to the molecular layer of the dentate gyrus [34]. It has been reported that the perforant pathway contributes 80%–85% of the synapses on the outer portion of the dendrites that arise from the dentate gyrus granule cells [34, 35]. The cells of origin of the perforant pathway in the entorhinal cortex are destroyed in the brain of patients with Alzheimer's disease [34]. Decreased binding potential of [^{11}C]MPDX in the medial temporal cortex is considered to be affected by insufficiency or damage to the perforant pathway in patients with Alzheimer's disease. Decreased binding potential of [^{11}C]MPDX in the temporal cortex in patients with Alzheimer's disease can be directly or indirectly correlated with destruction of the cells of origin of the perforant pathway. Thalamic nuclei have strong reciprocal connections with the cerebral cortex, forming thalamo-cortico-thalamic circuits. An abnormal finding in the thalamus of Alzheimer's disease has been described in a few MRI reports [36, 37]. It is considered that decreased binding potential of [^{11}C]MPDX in the thalamus is derived from corticothalamic transmission from the temporal and medial temporal cortices. The reason for the laterality in [^{11}C]MPDX and FDG-PET can be derived from investigations of small numbers ($n = 6$) of patients. Laterality in FDG-PET was also reported in a study with a small number of patients with Alzheimer's disease [38]. It is necessary to investigate these issues in greater number of patients.

We calculated the binding potential as a reference for the cerebellar cortex because the cerebellar cortex showed very low adenosine A_1 receptor densities [39] and this method provided well-balanced data in our earlier study [28]. The calculated binding potential of [^{11}C]MPDX in the medial temporal cortex was slightly lower than 0, which means that adenosine A_1 receptor density in the

medial temporal cortex in patients with Alzheimer's disease is nearly equal to or lower than that in the cerebellar cortex which contains very low adenosine A_1 receptor densities [39]. A severely decreased binding potential of [^{11}C]MPDX in the medial temporal cortex means that the perforant pathway in the medial temporal cortex is markedly insufficient or damaged in patients with Alzheimer's disease.

We consider that the decreased binding potential of [^{11}C]MPDX in the temporal and medial temporal cortices directly or indirectly reflects insufficiency or damage to the perforant pathway. On the other hand, the SPM analysis of FDG-PET findings in the present study revealed that FDG uptake was decreased in the temporal cortex and not in the medial temporal cortex, where the binding potential of [^{11}C]MPDX decreased markedly. The findings suggested that insufficiency or damage to the perforant pathway in the medial temporal cortex could not necessarily be reflected by the FDG-PET results.

Hypometabolism in the temporo-parietal cortex and posterior cingulate gyrus (Fig. 3b) is a typical pattern revealed by FDG-PET in Alzheimer's disease subjects [23–25, 40, 41]. In the temporo-parietal cortex, the area with severe hypometabolism was obviously larger than that with decreased binding potential of [^{11}C]MPDX in patients with Alzheimer's disease. In the posterior cingulate gyrus, [^{11}C]MPDX PET was not coupled with hypometabolism. Therefore, FDG-PET is more sensitive in detecting the degeneration of the temporo-parietal cortex and posterior cingulate gyrus, which is a typical manifestation in Alzheimer's disease, than [^{11}C]MPDX PET. However, it is well known that FDG-PET in Alzheimer's disease does not necessary reflect the pathological changes [42–44]. [^{11}C]MPDX PET provides a different diagnostic tool than FDG-PET, and could be valuable in detecting the degeneration in the medial temporal cortex. In addition, [^{11}C]MPDX PET has the possibility to detect corticothalamic transmission from the temporal and medial temporal cortices.

Conclusions

In patients with Alzheimer's disease, the binding potential of [^{11}C]MPDX decreased significantly in the temporal and medial temporal cortices and thalamus, and a small or no decrease was observed in the parietal cortex and posterior cingulate gyrus. The pattern of the binding potential of [^{11}C]MPDX had the possibility to be different from that of the FDG-PET in patients with Alzheimer's disease.

Acknowledgments This work was supported by Grants-in-Aid for Scientific Research (B) Nos. 16390348 and 20390334 from the Japan Society for the Promotion of Science. The authors thank Dr. Kazunori Kawamura for the preparation of [^{11}C]MPDX and Ms. Miyoko Ando for her care of the subjects during the PET measurement.

References

1. Dunwiddie TV, Masino SA. The role and regulation of adenosine in the central nervous system. Ann Rev Neurosci 2001; 24:31–55.
2. Yacoubi ME, Costentin J, Vaugeois JM. Adenosine A_{2A} receptors and depression. Neurology 2003;61:S82–7.
3. von Lubitz DK. Adenosine in the treatment of stroke: yes, maybe, or absolutely not? Expert Opin Investig Drugs 2001; 10:619–32.
4. Haas HL, Selbach O. Functions of neuronal adenosine receptors. Naunyn Schmiedebergs Arch Pharmacol 2000;362: 375–81.
5. Collis MG, Hourani SMO. Adenosine receptor subtypes. Trends Pharmacol Sci 1993;14:360–6.
6. Fredholm BB, Abbracchio MP, Burnstock G, Daly JW, Harden TK, Jacobson KA, et al. Nomenclature and classification of purinoceptors. Pharmacol Rev 1994;46:143–56.
7. Corradetti R, Lo Conte G, Moroni F, Passani MB, Pepeu G. Adenosine decreases aspartate and glutamate release from rat hippocampal slices. Eur J Pharmacol 1984;104:19–26.
8. Dolphin AC, Archer ER. An adenosine agonist inhibits and a cyclic AMP analogue enhances the release of glutamate but not GABA from slices of rat dentate gyrus. Neurosci Lett 1983;43:49–54.
9. Dunwiddie TV. The physiological role of adenosine in the central nervous system. Int Rev Neurobiol 1985;27:63–139.
10. Fredholm BB, Dunwiddie TV. How does adenosine inhibit transmitter release? Trends Pharmacol Sci 1988;9:130–4.
11. Fredholm BB, Hedqvist P. Modulation of neurotransmission by purine nucleotides and nucleosides. Biochem Pharmacol 1980;29:1635–43.
12. Phillis JW, Wu PH. The role of adenosine and its nucleotides in central synaptic transmission. Prog Neurobiol 1981;16: 187–239.
13. Schoenberg BS. Epidemiology of Alzheimer's disease and other dementing disorders. J Chronic Dis 1986;39:1095–104.
14. Fratiglioni L, Grut M, Forsell Y, Viitanen M, Grafstrom M, Holmen K, et al. Prevalence of Alzheimer's disease and other dementias in an elderly urban population: relationship with age, sex, and education. Neurology 1991;41:1886–92.
15. Brookmeyer R, Gray S, Kawas C. Projections of Alzheimer's disease in the United States and the public health impact of delaying disease onset. Am J Public Health 1998;88:1337–42.
16. Weinberger M, Gold DT, Divine GW, Cowper PA, Hodgson LG, Schreiner PJ, et al. Expenditures in caring for patients with dementia who live at home. Am J Public Health 1993; 83:338–41.
17. Osttbye T, Crosse E. Net economic costs of dementia in Canada. CMAJ 1994;151:1457–63.
18. Ernst R, Hay JW, Fenn C, Tinklenberg J, Yesavage JA. Cognitive function and the costs of Alzheimer's disease. Arch Neurol 1997;54:687–93.
19. Jansen K, Faull RLM, Dragunow M, Synek BJL. Alzheimer's disease: changes in hippocampal *N*-methyl-D-aspartate, quisqualate, neurotensin, adenosine, benzodiazepine, sero-

tonin and opioid receptors: an autoradiographic study. Neuroscience 1990;39:613–27.
20. Ulas J, Brunner LC, Nguyen L, Cotman CW. Reduced density of adenosine A1 receptors and preserved coupling of adenosine A1 receptors to G proteins in Alzheimer hippocampus: a quantitative autoradiographic study. Neuroscience 1993;52: 843–54.
21. Jaarsma D, Sebens B, Korf J. Reduction of adenosine A1-receptors in the perforant pathway terminal zone in Alzheimer hippocampus. Neurosci Lett 1991;121:111–4.
22. Kalaria RN, Sromek S, Wilcox BJ, Unnerstall JR. Hippocampal adenosine A1 receptors are decreased in Alzheimer's disease. Neurosci Lett 1990;118:257–60.
23. Ishii K, Sasaki H, Kono AK, Miyamoto N, Fukuda T, Mori E. Comparison of gray matter and metabolic reduction in mild Alzheimer's disease using FDG-PET and voxel-based morphometric MR studies. Eur J Nucl Med 2005;32:959–63.
24. Mosconi L. Brain glucose metabolism in the early and specific diagnosis of Alzheimer's disease. FDG-PET studies in MCI and AD. Eur J Nucl Med 2005;32:486–510.
25. Meguro K, LeMestric C, Landeau B, Desgranges B, Eustache F, Baron JC. Relations between hypometabolism in the posterior association neocortex and hippocampal atrophy in Alzheimer's disease: a PET/MRI correlative study. J Neurol Neurosurg Psychiatry 2001;71:315–21.
26. Fukumitsu N, Ishii K, Kimura Y, Oda K, Sasaki T, Mori Y, et al. Imaging of adenosine A_1 receptors in the human brain by positron emission tomography with [^{11}C]MPDX. Ann Nucl Med 2003;17:511–5.
27. Fukumitsu N, Ishii K, Kimura Y, Oda K, Sasaki T, Mori Y, et al. Adenosine A_1 receptor mapping of the human brain by PET with 8-dicyclopropylmethyl-1-11C-methyl-3-propylxanthine. J Nucl Med 2005;46:32–7.
28. Kimura Y, Ishii K, Fukumitsu N, Oda K, Sasaki T, Kawamura K, et al. Quantitative analysis of adenosine A_1 receptors in human brain using positron emission tomography and [1-methyl-^{11}C]8-dicyclopropylmethyl-1-methyl-3-propylxanthine. Nucl Med Biol 2004;31:975–81.
29. Naganawa M, Kimura Y, Nariai T, Ishii K, Oda K, Manabe Y, et al. Omission of serial arterial blood sampling in neuroreceptor imaging with independent component analysis. Neuroimage 2005;26:885–90.
30. Zigmond AS, Snaith RP. The Hospital Anxiety and Depression Scale. Acta Psychiatr Scand 1983;67:361–7.
31. Noguchi J, Ishiwata K, Furuta R, Simada J, Kiyosawa M, Ishii S, et al. Evaluation of carbon-11 labeled KF15372 and its ethyl and methyl derivatives as a potential CNS adenosine A_1 receptor ligand. Nucl Med Biol 1997;24:53–9.
32. Ishiwata K, Nariai T, Kimura Y, Oda K, Kawamura K, Ishii K, et al. Preclinical studies on [^{11}C]MPDX for mapping adenosine A_1 receptors by positron emission tomography. Ann Nucl Med 2002;16:377–82.
33. Ardekani BA, Braun M, Hutton BF, Kanno I, Iida H. A fully automatic multimodality image registration algorithm. J Comput Assist Tomog 1995;19:615–23.
34. Dragunow M, Murphy K, Leslie RA, Robertson HA. Localization of adenosine A1-receptors to the terminals of the perforant path. Brain Res 1988;462:252–7.
35. Hyman BT, Van Hoesen GW, Kromer LJ, Damasio AR. Perforant pathway changes and the memory impairment of Alzheimer's disease. Ann Neurol 1986;20:472–81.
36. Stephen RE, Janke AL, Chark JB. Gray and white matter changes in Alzheimer's disease: a diffusion tensor imaging study. J Magn Reson Imaging 2008;27:20–6.
37. Medina D, DeToledo-Morrell L, Urresta F, Gabrieli JD, Moseley M, Fleischman D, et al. White matter changes in mild cognitive impairment and AD: a diffusion tensor imaging study. Neurobiol Aging 2006;27:663–72.
38. Zahn R, Juengling F, Bubrowski P, Jost E, Dykierek P, Talazko J, et al. Hemisphere asymmetries of hypometabolism associated with semantic memory impairment in Alzheimer's disease: a study using positron emission tomography with fluorodeoxygulcose-F18. Psychiatry Res Neuroimaging 2004; 132:159–72.
39. Fastbom J, Pazos A, Probst A, Palacios JM. Adenosine A1 receptors in the human brain: a quantitative autoradiographic study. Neuroscience 1987;22:827–39.
40. Sakamoto S, Ishii K, Sasaki M, Hosaka M, Mori T, Matsui M, et al. Differences in cerebral metabolic impairment between early and late onset types of Alzheimer's disease. J Neurol Sci 2002;15:27–32.
41. Kim EJ, Cho SS, Jeong Y, Park KC, Kang E, Kim SE, et al. Glucose metabolism in early onset versus late onset Alzheimer's disease: an SPM analysis of 120 patients. Brain 2005;128:1790–801.
42. Ibanez V, Pietrini P, Alexander GE, Furey ML, Teichberg D, Rajapakse JC, et al. Regional glucose metabolic abnormalities are not the result of atrophy in Alzheimer's disease. Neurology 1998;50:1585–93.
43. Mosconi L, Sorbi S, de Leon MJ, Li Y, Nacmias B, Myoung PS, et al. Hypometabolism exceeds atrophy in presymptomatic early-onset familial Alzheimer's disease. J Nucl Med 2006;47:1778–86.
44. Chetelat G, Desgranges B, Landeau B, Mezenge F, Poline JB, de la Sayette V, et al. Direct voxel-based comparison between grey matter hypometabolism and atrophy in Alzheimer's disease. Brain 2008;131:60–71.

Ann Nucl Med (2008) 22:191–200
DOI 10.1007/s12149-007-0099-7

ORIGINAL ARTICLE

Influence of mild hyperglycemia on cerebral FDG distribution patterns calculated by statistical parametric mapping

Keiichi Kawasaki · Kenji Ishii · Yoko Saito
Keiichi Oda · Yuichi Kimura · Kiichi Ishiwata

Received: 2 October 2007 / Accepted: 29 November 2007

Abstract
Objective In clinical cerebral 2-[^{18}F]fluoro-2-deoxy-D-glucose positron emission tomography (FDG-PET) studies, we sometimes encounter hyperglycemic patients with diabetes mellitus or patients who have not adhered to the fasting requirement. The objective of this study was to investigate the influence of mild hyperglycemia (plasma glucose range 110–160 mg/dl) on the cerebral FDG distribution patterns calculated by statistical parametric mapping (SPM).
Methods We studied 19 healthy subjects (mean age 66.2 years). First, all the subjects underwent FDG-PET scans in the fasting condition. Then, 9 of the 19 subjects (mean age 64.3 years) underwent the second FDG-PET scans in the mild hyperglycemic condition. The alterations in the FDG-PET scans were investigated using SPM- and region of interest (ROI)-based analyses. We used three reference regions: (1) SPM global brain (SPMgb) used for SPM global mean calculation, (2) the gray and white matter region computed from magnetic resonance image (MRIgw), and (3) the cerebellar cortex (Cbll).
Results The FDG uptake calculated as the standardized uptake value (average) in SPMgb, MRIgw, and Cbll regions in the mild hyperglycemic condition was 42.7%, 41.3%, and 40.0%, respectively, of that observed in the fasting condition. In SPM analysis, the mild hyperglycemia was found to affect the cerebral distribution patterns of FDG. The FDG uptake was relatively decreased in the gray matter, mainly in the frontal, temporal, and parietal association cortices, posterior cingulate, and precuneus in both SPMgb- and MRIgw-reference-based analyses. When Cbll was adopted as the reference region, those decrease patterns disappeared. The FDG uptake was relatively increased in the white matter, mainly in the centrum semiovale in all the reference-based analyses.
Conclusions It is noteworthy that the FDG distribution patterns were altered under mild hyperglycemia in SPM analysis. The decreased uptake patterns in SPMgb- (SPM default) and MRIgw-reference-based analyses resembled those observed in Alzheimer's disease. Under mild hyperglycemia, we can recommend Cbll as the reference region to detect decreased uptake patterns. We should pay special attention to controlling the diet condition, monitoring hyperglycemia, and optimizing the reference region in SPM analysis, particularly in the diagnosis of early Alzheimer's disease in clinical FDG-PET.

Keywords FDG-PET · Mild hyperglycemia · Distribution pattern · Statistical parametric mapping · Alzheimer's disease

Introduction

Cerebral 2-[^{18}F]fluoro-2-deoxy-D-glucose positron emission tomography (FDG-PET) examinations are widely used for the diagnosis of neurological disorders such as dementia, epilepsy, and tumors. A high plasma glucose level and diet-enhanced FDG uptake by extra-brain tissues decrease the FDG uptake in the brain and reduce the quality of brain images [1, 2]. So the examinations

K. Kawasaki (✉) · K. Ishii · Y. Saito · K. Oda · Y. Kimura · K. Ishiwata
Positron Medical Center, Tokyo Metropolitan Institute of Gerontology, 1-1 Naka-cho, Itabashi-ku, Tokyo 173-0022, Japan
e-mail: kawasaki@pet.tmig.or.jp

are usually carried out after a 4–6-h fast to give a low plasma glucose concentration. However, FDG-PET is sometimes carried out in hyperglycemic patients with diabetes mellitus, or in patients who have not adhered to the fasting requirement. Nevertheless, in most cases, the glucose level is still less than the criterion of hyperglycemia (plasma glucose > 160 mg/dl) as described in the "European Association of Nuclear Medicine Procedure Guidelines for Brain Imaging using [^{18}F]FDG" [2]. In such mild hyperglycemic cases, it is usually assumed that the FDG distribution pattern in the brain in the fasting condition is maintained regardless of plasma glucose levels.

In recent years, clinical examinations require the detection of subtle abnormalities of regional cerebral FDG uptake in patients with neurological disorders such as early Alzheimer's disease and refractory focal epilepsy. Usually, static (semi-quantitative) images of FDG are used, and when data from age-matched normal controls are available, the data from each patient are evaluated by statistical approaches such as statistical parametric mapping (SPM) [3] and three-dimensional (3D) stereotactic surface projection (3D-SSP) techniques [4].

In the course of the SPM analysis in the FDG-PET studies, we have encountered patients who had not fasted but whose plasma glucose level was no more than 160 mg/dl. However, the results of the SPM analysis sometimes showed abnormalities different from the clinical presentation.

With regard to the relationship between cerebral glucose metabolism and the plasma glucose level, Hasselbalch et al. [6] measured the global cerebral metabolic rate of glucose (CMRglc) and regional CMRglc (rCMRglc) on the basis of the Sokoloff model [5] in normoglycemic control condition (plasma glucose 97 mg/dl) and in an acute hyperglycemic condition (270 mg/dl) in six normal subjects. They reported that during acute hyperglycemia, when compared with the normoglycemia, with the exception of a significant increase (42%) in the white matter in the centrum semiovale, the global CMRglc and rCMRglc in the cortical and subcortical gray matter regions did not change. However, if a significant increase occurs unexpectedly in the white matter in the centrum semiovale during hyperglycemia, as demonstrated by Hasselbalch et al. [6], the subjects whose plasma glucose level is not controlled to the fasting level may be erroneously diagnosed by the statistical approaches. Therefore, it is necessary to investigate whether the plasma glucose levels alter the regional cerebral FDG uptake, thereby possibly influencing the FDG distribution patterns obtained by using the statistical approaches.

In the present study, we focused on the glucose levels less than the aforementioned criterion of hyperglycemia (>160 mg/dl) [2]. As a fasting glucose level from 70 mg/dl to 109 mg/dl in plasma is generally considered to be normal, we defined the plasma glucose level from 110 mg/dl to 160 mg/dl as mild hyperglycemia.

The objective of this study was to investigate the influence of plasma glucose levels within the mild hyperglycemia on the cerebral FDG distribution patterns, particularly the patterns obtained by using SPM analysis.

Materials and methods

Subjects and conditions

We studied 19 healthy subjects (6 men and 13 women) with a mean age of 66.2 years (range 48–80 years). All the subjects fulfilled the following criteria: (1) no history of diabetes mellitus, neurological or psychiatric disorders, head trauma, drug abuse, alcoholism, hypertension, or cardiac disease, (2) no medication, (3) found to be normal on physical and neurological examinations, (4) Mini-Mental State Examination score = 30, and (5) found to be normal on anatomical magnetic resonance imaging (MRI), i.e., 3D-MRI (described below) and T2-weighted MRI. This study was approved by the institutional Ethics Committee. A written informed consent was obtained from all the subjects before the study.

First all the subjects underwent FDG-PET scanning in the fasting condition (after >5-h fasting). Then, within 1 month, 9 of the 19 subjects (2 men and 7 women, mean age 64.3 years, range 48–80 years) underwent a second FDG-PET scanning in the mild hyperglycemic condition in which each subject first consumed a normal lunch 2–2.5 h prior to the FDG injection and was then orally administered 50 g glucose (TRELAN-G50, 150 ml; Ajinomoto Pharma, Tokyo, Japan) 30 min prior to the FDG injection. At PET measurement 1–2 ml of venous blood samples were drawn twice immediately prior to the intravenous FDG injection and 30 min following the injection (t = 0 min and 30 min, respectively), and the plasma glucose concentration was measured. The paired comparison between the fasting and mild hyperglycemic conditions was done using the data obtained from the 9 subjects scanned twice, and the comparisons between one scan in the fasting or hyperglycemic condition and the normal database were done between the data obtained from the 9 subjects and the data of the 19 subjects in the fasting condition.

Image acquisition

For all subjects, the 3D-MRI images with T1-weighted contrast were obtained with a 1.5-T Sigma Horizon scanner (GE, Milwaukee, WI, USA) using the following imaging parameters: matrix size 256 × 256 × 124 and voxel size 0.9375 × 0.9375 × 1.3 mm. The images were obtained using the 3D spoiled gradient echo protocol (TR/TE = 9.2 ms/2.0 ms) before the first FDG-PET scan.

FDG images were obtained with a PET scanner (SET 2400W; Shimadzu, Kyoto, Japan) in the 3D mode [image resolution: transverse full width at half-maximum (FWHM) = 4.4 mm, axial FWHM = 6.5 mm]. Forty-five minutes following the intravenous injection of FDG (130.4 ± 15.0 MBq), a 6-min emission scan was collected to create images with the following parameters: matrix size 128 × 128 × 50 and voxel size 2 × 2 × 3.125 mm. The attenuation was corrected by a transmission scan using a ^{68}Ga/^{68}Ge source. During the tracer-accumulation phase, the subjects remained supine, quiet, and motionless in a dimly lit and quiet (except for air-conditioner noise) room with their eyes open and ears unoccluded.

Image processing

Image processing and data analysis were performed using SPM2 (Functional Imaging Laboratory, London, UK) implemented on MATLAB (The MathWorks, Natick, MA, USA) and Dr. View (AJS, Tokyo, Japan). The tasks performed by SPM2 were MRI/PET coregistration, spatial normalization, spatial smoothing, MRI segmentation, normalization for reference region, and SPM analysis. The tasks performed by Dr. View were image masking and region of interest (ROI) analysis. All FDG images were spatially normalized and resampled (XYZ matrix 79 × 95 × 80 and voxel size 2 × 2 × 2 mm) using the FDG template which was created from the FDG images of 15 physically and psychiatrically healthy subjects (mean age 33.3 years, range 20–49 years) in accordance with a method described elsewhere [7]. Each 3D-MRI image was coregistered to the corresponding FDG image in the fasting condition and normalized to the FDG template using the parameters obtained from the spatial normalization of the corresponding FDG images.

To investigate alterations of regional FDG uptake and FDG distribution patterns, we used three kinds of image reference regions termed as SPMgb, MRIgw, and Cbll (Fig. 1). SPMgb (Fig. 1b) indicates the SPM global brain region used for the calculation of global mean in default in SPM program. SPMgb is defined implicitly in each image by using a two-step process: first the overall mean is computed, and then voxels measuring less than the quotient of the mean divided by 8 are deemed extracranial and are masked out. Thus, SPMgb is uniquely defined image-by-image. The global mean is then recomputed on the remaining voxels. MRIgw (Fig. 1c) indicates an MRI-based gray and white matter region computed using the segmentation function of SPM program and is defined for each subject separately. Cbll

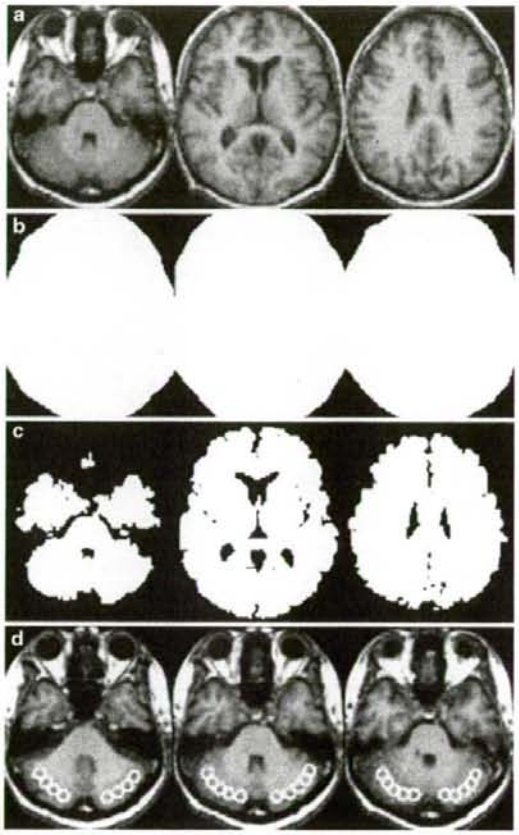

Fig. 1 An example of the brain regions investigated. **a** The space normalized 3D-magnetic resonance imaging (MRI) image of a subject. **b** Statistical parametric mapping global brain (SPMgb) computed from the 2-[^{18}F]fluoro-2-deoxy-D-glucose positron emission tomography (FDG-PET) image of the subject in the fasting condition in default in SPM program (smoothed using a Gaussian filter with a 16-mm full width at half-maximum). SPMgb in the mild hyperglycemic condition was nearly equal to that in the fasting condition (not shown). **c** MRIgw consisting of the gray and white matter regions computed from the 3D-MRI image of the subject using SPM segmentation function. **d** Cerebellar cortex [Cbll, region of interest (ROI) on cerebellar cortex] consisting of 48 circles 10 mm in diameter on five continuous slices

(Fig. 1d) indicates the ROI on the cerebellar cortex common to all spatially normalized images. It is noted that the MRIgw includes gray and white matter regions, whereas the SPMgb contains the entire intracranial contents including cerebrospinal fluid and orbit regions.

The subject mean of SPMgb, MRIgw, and Cbll of each FDG image after spatial normalization was normalized to be 50 to create SPMgb- MRIgw-, and Cbll-reference-based images.

Data analysis

Regional uptake of the FDG

The FDG uptake in SPMgb, MRIgw, and Cbll in each scan for each subject scanned twice was expressed as the standardized uptake value [SUV, body weight (g) × tissue concentration (Bq/ml)/total injected dose (Bq)]. We performed the paired Wilcoxon t test comparing the FDG uptake (SUV) in the three reference regions between the two scans; $P < 0.01$ was considered to be significant.

SPM-based analysis of the FDG uptake

We performed three global normalization processes on the basis of SPMgb-, MRIgw-, and Cbll-reference-based images. Those images were smoothed using a Gaussian filter with a 16-mm FWHM to increase the sensitivity and then we calculated the statistical parametric maps of the paired t test between the first and second scans of the subjects scanned twice by the "Population main effect: 2 cond's, 1 scan/cond" of SPM analysis design type ($P < 0.001$, uncorrected, extent threshold $k = 300$ voxels). We also calculated the statistical maps using "Compare-populations: 1 scan/subject (Ancova)" with age as a covariate between each scan in the fasting or mild hyperglycemic condition of the 9 subjects and the scans in the fasting condition of the other 18 of the 19 subjects (1 of the 19 subjects under comparison was excluded) using it as the normal database ($P < 0.01$, uncorrected, extent threshold $k = 300$ voxels).

ROI-based analysis of the FDG uptake

In the subjects scanned twice, the ROIs common to all normalized images were placed on the Cbll, centrum semiovale, and the frontal, temporal, and parietal cortices, and posterior cingulate/precuneus. The ROIs of the Cbll, centrum semiovale, and the frontal, temporal, and parietal cortices, and posterior cingulate/precuneus consisted of 48 circles 10 mm in diameter on 5 continuous slices, 26 on 5, 116 on 16, 116 on 17, 50 on 7, and 46 on 17, respectively. The relative FDG uptake in the ROIs was calculated in SPMgb-, MRIgw-, and Cbll-reference-based images without smoothing. For the ROI-based statistical analysis, the paired Wilcoxon t test was performed for each of the six ROIs between two scans; $P < 0.05$ with Bonferroni correction (total number of comparisons = 6, new alpha level = 0.0083) was considered to be significant.

Results

Fasting and mild hyperglycemic conditions

The plasma glucose concentration was significantly increased in the mild hyperglycemic condition: fasting scan (19 subjects), 91.7 ± 4.6 mg/dl at $t = 0$ min and 90.8 ± 5.5 mg/dl at $t = 30$ min; fasting scan (9 subjects scanned twice within 19 subjects), 90.0 ± 4.4 mg/dl at $t = 0$ min and 90.9 ± 6.9 mg/dl at $t = 30$ min; and mild hyperglycemic scan (9 subjects), 136.1 ± 10.5 mg/dl at $t = 0$ min, 138.1 ± 14.0 mg/dl at $t = 30$ min.

Three image reference regions and the FDG uptake

Figure 1 represents the space normalized 3D-MRI image of a subject and the three defined image reference regions (SPMgb, MRIgw, and Cbll). The SPMgb regions in both the fasting and mild hyperglycemic conditions were nearly equal.

The FDG uptake (SUV) in the three reference regions decreased greatly in the mild hyperglycemic condition ($P < 0.01$, Fig. 2). The SUV values in the SPMgb, MRIgw, and Cbll in the mild hyperglycemic condition were 42.7%, 41.3%, and 40.0%, respectively, of those observed in the fasting condition.

Paired comparison between the fasting and mild hyperglycemic conditions

First, the paired t test between the fasting and mild hyperglycemic conditions was performed by SPM, and the results are shown in Fig. 3 ($P < 0.001$, uncorrected, $k = 300$). In the contrast "uptake in the mild hyperglycemic condition < uptake in the fasting condition (uptake in M.hygl < uptake in Fasting)", the uptake in the gray matter and cerebellar cortex regions greatly decreased in SPMgb-reference-based analysis (Fig. 3a), and clear decreases were detected in the frontal, temporal, and parietal cortices, posterior cingulate, and precuneus in MRIgw-reference-based analysis (Fig. 3b). However, no decreased uptake pattern was detected in Cbll-reference-based analysis (not shown). In the contrast "uptake in

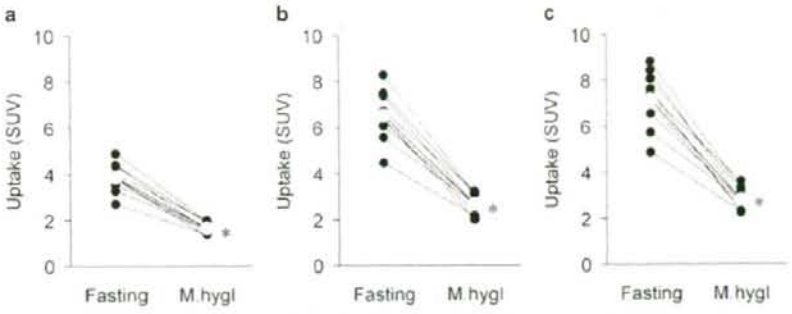

Fig. 2 FDG uptake (standardized uptake value) in SPMgb (**a**), MRIgw (**b**), and Cbll (**c**), respectively. The uptake was compared in the nine subjects scanned twice in the fasting and mild hyperglycemic (M.hygl) conditions. *Solid circles* represent individual subjects, and *open circles* represent the average ($n = 9$). $^*P < 0.01$ (paired Wilcoxon t test)

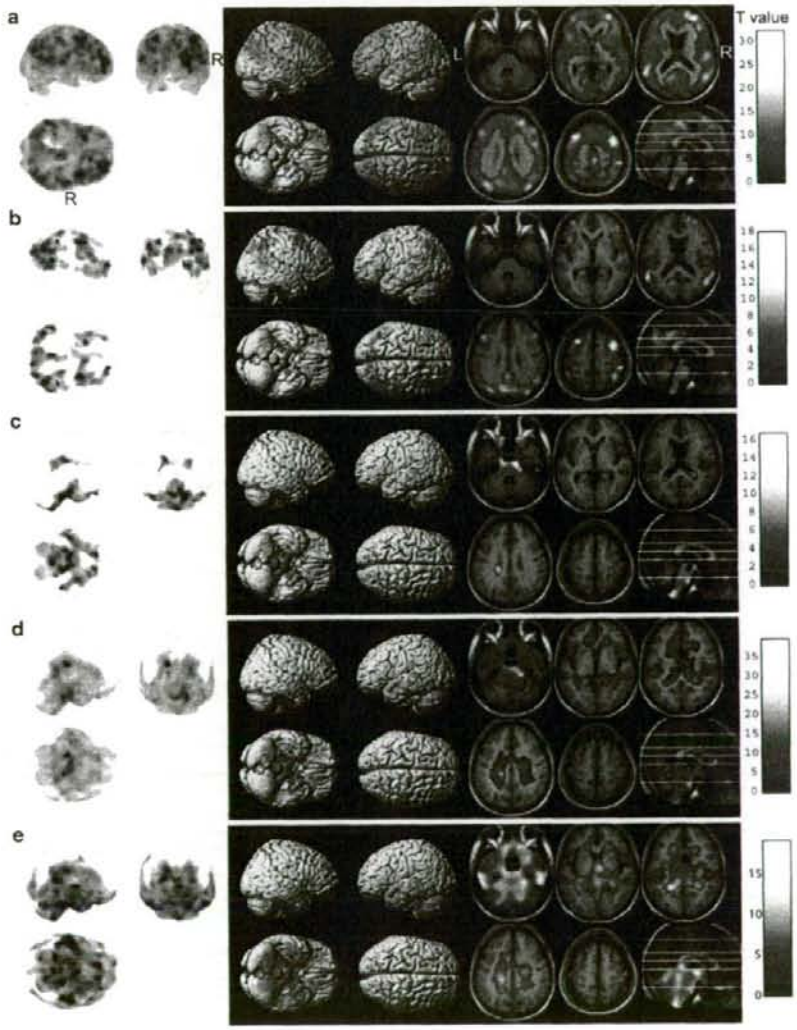

Fig. 3 SPM paired t tests "uptake in M.hygl < uptake in Fasting" in SPMgb- (**a**) and MRIgw- (**b**) reference-based analyses, and "uptake in M. hygl > uptake in Fasting" in SPMgb- (**c**), MRIgw- (**d**), and Cbll- (**e**) reference-based analyses. No decreased uptake pattern was detected in the mild hyperglycemic condition in Cbll-reference-based analysis (not shown). The SPM paired t tests were performed in the nine subjects scanned twice in the fasting and mild hyperglycemic conditions ($P < 0.001$, uncorrected; $k = 300$)

the mild hyperglycemic condition > uptake in the Fasting condition (uptake in M.hygl > uptake in Fasting)", the uptake increased in the centrum semiovale and cerebrospinal fluid regions in SPMgb-reference-based analysis (Fig. 3c), whereas significant increases were revealed in the white matter, cerebellar medullary substance, and cerebrospinal fluid regions in MRIgw- and Cbll-reference-based analyses (Fig. 3d, e).

Second, ROI-based analysis was performed for the FDG uptake in the six regions in both the fasting and mild hyperglycemic conditions in SPMgb-, MRIgw-, and Cbll-reference-based images. In the mild hyperglycemic condition, the uptake significantly decreased in the frontal (9.9%), temporal (7.6%), and parietal (9.2%) cortices, posterior cingulate/precuneus (9.9%), and Cbll (7.8%) in SPMgb-reference-based images (Fig. 4a), and in the frontal (5.6%) and temporal (3.2%) cortices, and posterior cingulate/precuneus (5.4%) in MRIgw-reference-based images (all $P<0.05$, Fig. 4b), but no decreased uptake ROI was revealed in Cbll-reference-based images (Fig. 4c). On the other hand, the uptake significantly increased in the centrum semiovale: 10.8%, 16.1%, and 20.1% in SPMgb- (Fig. 4a), MRIgw- (Fig. 4b), and Cbll- (Fig. 4c) reference-based images, respectively (all $P < 0.05$).

Comparison between one scan in the fasting or mild hyperglycemic condition and the normal database

"Compare-populations: 1 scan/subject (Ancova)" with age as a covariate between each scan in the fasting or mild hyperglycemic condition of the 9 subjects and the scans in the fasting condition of the other 18 of the 19 subjects was performed by SPM, and the results in the contrast "uptake of one scan < uptake of the normal database" are shown on the sagittal projection in Fig. 5 ($P < 0.01$, uncorrected, $k = 300$). In the fasting condition, no notably decreased uptake pattern in common with nine subjects was detected in SPMgb-reference-based analysis (Fig. 5a). The spots observed in subjects 1, 4, 6, 7, and 9 were considered to be derived from individual morphological deviations that were not completely fitted to the FDG-PET template when compared with MRI images of each subject. In the mild hyperglycemic condition, significant decreases were observed in the association cortices such as frontal, temporal, and parietal cortices, posterior cingulate, and precuneus in SPMgb-reference-based analysis (Fig. 5b). The regions showing decreased uptake were greatly reduced in MRIgw-reference-based analysis, but the decreases were observed in the association cortices, posterior cingulate, and precuneus in some subjects (Fig. 5c). However, no decreased uptake patterns in any subjects were revealed in Cbll-reference-based analysis (not shown).

The results in the contrast "uptake of one scan > uptake of the normal database" were as follows (figures not shown). In the fasting condition, no notably increased uptake in common with nine subjects was detected. In the mild hyperglycemic condition, slight increases were observed in the white matter, cerebellar medullary substance, and cerebrospinal fluid regions in SPMgb-reference-based analysis in some subjects. The regions showing increased uptake spread widely in MRIgw- and Cbll-reference-based analyses.

Discussion

It is well known that a high plasma glucose concentration globally reduces FDG uptake in the brain [1, 2]. In this study, we confirmed that mild hyperglycemia (plasma glucose levels from 110 mg/dl to 160 mg/dl) decreased the FDG uptake in the SPMgb, MRIgw, and Cbll regions to 42.7%, 41.3%, and 40.0% of that in the fasting condition, respectively (Fig. 2).

Regarding the FDG distribution patterns calculated by SPM, we obtained the following findings. The mild hyperglycemia relatively decreased the FDG uptake in the gray matter in both SPMgb- and MRIgw-reference-based analyses (Figs. 3a, b, 4b, c). It should be noted that the regions showing relatively decreased uptake were the frontal, temporal, and parietal association cortices, posterior cingulate, and precuneus. It is well recognized that rCMRglc decreases in these association cortices are observed in Alzheimer's disease [8–12], and the decrease in the posterior cingulate and precuneus is considered to be an early sign of this disorder [13, 14]. Therefore, these findings demonstrate the possibility that SPMgb- or MRIgw-reference-based SPM analysis in FDG-PET could erroneously diagnose normal subjects whose plasma glucose levels were not below 110 mg/dl as patients with the early stages of Alzheimer's disease. However, the mild hyperglycemia did not reveal any decreases of FDG uptake in Cbll-reference-based analysis. Considering this result, we can recommend Cbll-reference-based analysis in the diagnosis of early Alzheimer's disease in the mild hyperglycemic condition. On the other hand, when we calculated the uptake increase regions in the mild hyperglycemic condition, the increases in the white matter, cerebellar medullary substance, and cerebrospinal fluid regions were detected, strongly, in MRIgw- and Cbll-reference-based analyses (Fig. 3c–e). Then, we realized that it would be difficult to detect increased uptake patterns characteristic of some degenerative diseases in SPM analysis in the mild hyperglycemic condition.

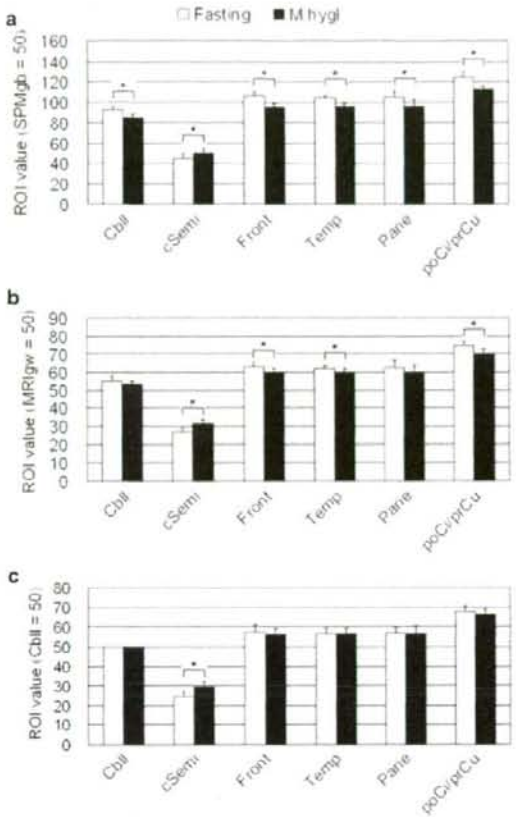

Fig. 4 Relative regional FDG uptake in the brain in the fasting and mild hyperglycemic (M.hygl) conditions in the SPMgb- (**a**), MRIgw- (**b**), and Cbll- (**c**) reference-based images. *Cbll* cerebellar cortex, *cSemi* centrum semiovale, *Front* frontal cortex, *Temp* temporal cortex, *Parie* parietal cortex, and *poCilprCu* posterior cingulate/precuneus. The region of interest (ROI) values are shown as mean and SD ($n = 9$). $^*P < 0.05$ (paired Wilcoxon t test with Bonferroni correction)

The most notable factor making a difference in the SPM results (T values) depending on the reference regions would be the difference in the relative amount of gray matter included in each reference region (Fig. 1). This is because the FDG uptake alterations induced by mild hyperglycemia in the gray matter and other regions were toward opposite directions: a decrease in the gray matter, but an increase in the white matter and extracerebral tissues (Figs. 3, 4).

Regarding the test–retest reproducibility of FDG-PET, several groups have confirmed that the global CMRglc and rCMRglc were reproducible, and the relative rCMRglc was more stable than the rCMRglc in the fasting condition within and among normal subjects with ages ranging from 23 years to 38 years in an ROI-based analysis [15–18]. Prior to the present study, we also confirmed the reproducibility of FDG-PET in the fasting condition within and among aged healthy subjects with ages ranging from 48 years to 80 years by the same method used in the present SPM-based analysis (unpublished data). The intrasubject test was done within 10 subjects, and the intersubject test was done between the 10 subjects and 9 subjects. The paired t test for the comparison within subjects and the two-sample t test for the comparison among subjects by SPM did not reveal variations in any of the normalization processes based on SPMgb, MRIgw, or Cbll ($P < 0.001$, uncorrected, $k = 300$).

In the FDG-PET study conducted by Hasselbalch et al. [6], the plasma glucose level (270 mg/dl) during hyperglycemia was approximately twice as high as that observed in the mild hyperglycemic condition (137 mg/dl) of the present study. In addition, the plasma glucose levels in their study were clamped by a constant infusion of somatostatin and insulin and variable intravenous infusions of 20% glucose. In terms of the glucose intake method, extrinsic factors of the brain (intravenous and passive intake of nutrients) were reflected in their study, but intrinsic factors (oral and spontaneous intake of nutrients) were reflected in our study. They reported that no global or regional difference in CMRglc was apparent during hyperglycemia, except for a significant increase in white matter in the centrum semiovale (42%). It is noted that Hasselbalch et al. [6] compared the quantitative CMRglc values in normal and hyperglycemic conditions, whereas we studied differences in distribution patterns by the SMP- and ROI-based analyses using relative data (Figs. 3, 4, 5). When we calculated the relative rCMRglc values normalized by the global CMRglc using the values reported in their article, the percentage rates of the relative decrease were 7.4% in the frontal cortex, 4.1% in the temporal cortex, and 8.4% in the parietal cortex, and the rate of the relative increase was calculated to be 30.6% in the centrum semiovale. It is speculated that their high glucose level induced much higher uptake in the centrum semiovale as compared with the present study: 30.6% versus 20.1% (Cbll-reference-based study, Fig. 4c). As the reason why they found no regional difference in rCMRglc values except for the significant increase in the centrum semiovale, we suspect that they compared quantitative CMRglc values between two conditions using ROI-based analysis. It would be of great interest if the paired t test of SPM using their CMRglc data provided results similar to ours in Fig. 3.

The following possible reasons can explain the phenomenon that FDG distribution patterns in the brain

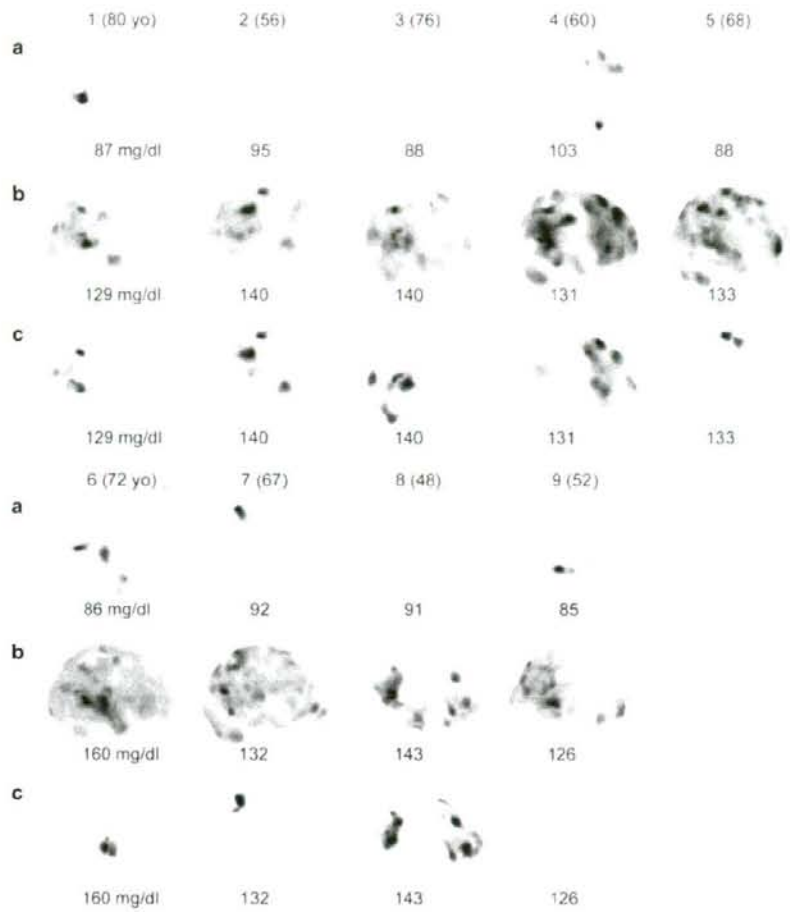

Fig. 5 SPM "Compare-populations: 1 scan/subject (Ancova)" with age as a covariate between each scan of the 9 subjects in the fasting or mild hyperglycemic condition and the scans of the other 18 of the 19 subjects in the fasting condition ($P < 0.01$, uncorrected, $k = 300$): "uptake of one scan in Fasting < uptake of the normal database" in SPMgb-reference-based analysis (**a**), and "uptake of one scan in M.hygl < uptake of the normal database" in SPMgb- (**b**) and MRIgw-reference-based analyses (**c**). No decreased uptake patterns in any subjects were revealed in Cbll-reference-based analysis (not shown). Subject numbers and ages in *parentheses* are presented on the top of three images of each subject and plasma glucose concentration (average) is presented at the bottom of each image

were regionally altered in the fasting and mild hyperglycemic conditions. (1) Difference in the cytoarchitecture that may cause a regional difference in the expression of glucose transporters and hexokinase and in turn may cause a regional difference in the lumped constant [5, 19, 20]. (2) The influence of the endocrine system, autonomic nervous system, psychological factors, or plasma glucose level related to the dietary condition may affect the regional cerebral function [6, 21, 22]. Regarding reason (1), the glucose transporter subtype 1 (GLUT1) is ubiquitously expressed in the brain, and the blood–brain barrier is a major site of its expression [23, 24]; on the other hand, the glucose transporter subtype 3 (GLUT3)—the predominant neuronal glucose transporter—is expressed in neurons [24, 25]. Asano et al. [26] had expressed the GLUT3 protein in Chinese hamster ovary (CHO) cells by the transfection of its cDNA by using an expression vector and compared its characteristics with those of the GLUT1 protein. A kinetic analysis revealed that the Michaelis constant (K_m) value of the GLUT3 protein for 3-*O*-methylglucose uptake in CHO cells was approximately 35% of that of GLUT1, whereas the K_m value of the GLUT3 protein for 2-deoxyglucose uptake was very similar to that of the GLUT1 protein. These data suggest the possibility that the regional differences in the expression ratios of GLUT1 and GLUT3 [27] and the heterogeneity of these transporters affect the FDG distribution patterns under mild hyperglycemia.

An epidemiological survey in Japan demonstrated that the frequency of diabetes mellitus diagnosed by the glucose tolerance test increased with age, with the frequency reaching 10–15% in elderly people aged 60 years or older with a high incidence of dementia [28]. In our institute these subjects sometimes undergo FDG-

PET for elucidating suspicious dementia, but the mild hyperglycemia makes it difficult to interpret the study properly. As a trial, we performed SPM "Compare-populations: 1 scan/subject (Ancova)" with age as a covariate between the FDG-PET scan of a 76-year-old subject with diabetes mellitus (plasma glucose 145 mg/dl) and mild cognitive impairment, and the 19 normal scans of the present study in SPMgb-, MRIgw-, and Cbll-reference-based analyses (unpublished data). We observed FDG distribution patterns that suggest Alzheimer's disease in the contrast "uptake of the patient < uptake of the normal database" in all reference-based analyses, but increase in the white matter in the contrast "uptake of the patient > uptake of the normal database" was not revealed in any reference-based analyses. The patient was then diagnosed with early Alzheimer's disease.

In conclusion, in the mild hyperglycemic condition, FDG uptake in the SPMgb, MRIgw, and Cbll regions was significantly decreased to 42.7%, 41.3%, and 40.0% of that in the fasting condition. It is noteworthy that FDG distribution patterns in SPMgb- (SPM default) and MRIgw-reference-based analyses were altered under mild hyperglycemia, and the decreased uptake patterns were fairly similar to those observed in Alzheimer's disease. However, when we adopted Cbll as the reference region, the decreased uptake patterns disappeared. We can recommend Cbll-reference-based analysis in the mild hyperglycemic condition to detect decreased uptake patterns. We should pay special attention to controlling the diet condition, monitoring hyperglycemia, and optimizing the reference region in SPM analysis, particularly in the diagnosis of early Alzheimer's disease in clinical FDG-PET.

Acknowledgments The authors are grateful to Drs. Hidenao Fukuyama, Kazuo Hashikawa, and Koichi Ishizu of Kyoto University for proper advice. We thank Drs. Kazunori Kawamura and Takashi Oda for the preparation of FDG and Ms. Miyoko Ando and Ms. Hiroko Tsukinari for nursing. We also thank Dr. Laurence Court for proofreading this manuscript. This research was partially supported by the Grants for Comprehensive Research Project on Longevity Science from the Ministry of Health, Labour and Welfare, Japan.

References

1. Vander Borght T, Laloux P, Maes A, Salmon E, Goethals I, Goldman S. Guidelines for brain radionuclide imaging: perfusion single photon computed tomography (SPECT) using Tc-99m radiopharmaceuticals and brain metabolism positron emission tomography (PET) using F-18 fluorodeoxyglucose. Acta Neurol Belg 2001;101:196–209.
2. Bartenstein P, Asenbaum S, Catafau A, Halldin C, Pilowski L, Pupi K, et al. European Association of Nuclear Medicine procedure guidelines for brain imaging using [^{18}F]FDG. Eur J Nucl Med Mol Imaging 2002;29:43–8.
3. Signorini M, Paulesu E, Friston K, Perani D, Colleluori A, Lucignani G, et al. Rapid assessment of regional cerebral metabolic abnormalities in single subjects with quantitative and nonquantitative [^{18}F]FDG PET: a clinical validation of statistical parametric mapping. Neuroimage 1999;9:63–80.
4. Minoshima S, Frey KA, Koeppe RA, Foster NL, Kuhl DE. A diagnostic approach in Alzheimer's disease using three-dimensional stereotactic surface projections of fluorine-18-FDG PET. J Nucl Med 1995;36:1238–48.
5. Sokoloff L, Reivich M, Kennedy C, Des Rosiers MH, Patlak CS, Pettigrew KD, et al. The [^{14}C]deoxyglucose method for the measurement of local cerebral glucose utilization: theory, procedure, and normal values in the conscious and anesthetized albino rat. J Neurochem 1977;28:897–916.
6. Hasselbalch SG, Knudsen GM, Capaldo B, Postiglione A, Paulson OB. Blood–brain barrier transport and brain metabolism of glucose during acute hyperglycemia in humans. J Clin Endocrinol Metab 2001;86:1986–90.
7. Meyer JH, Gunn RN, Myers R, Grasby PM. Assessment of spatial normalization of PET ligand images using-specific templates. Neuroimage 1999;9:545–53.
8. Benson DF, Kuhl DE, Hawkins RA, Phelps ME, Cummings JL, Tsai SY. The fluorodeoxyglucose 18F scan in Alzheimer's disease and multi-infarct dementia. Arch Neurol 1983;40:711–4.
9. Friedland RP, Brun A, Budinger TF. Pathological and positron emission tomographic correlations in Alzheimer's disease. Lancet 1985;1:228.
10. Duara R, Grady C, Haxby J, Sundaram M, Cutler NR, Heston L, et al. Positron emission tomography in Alzheimer's disease. Neurology 1986;36:879–87.
11. Rapoport SI, Horwitz B, Grady CL, Haxby JV, DeCarli C, Schapiro MB. Abnormal brain glucose metabolism in Alzheimer's disease, as measured by position emission tomography. Adv Exp Med Biol 1991;291:231–48.
12. Fukuyama H, Ogawa M, Yamauchi H, Yamaguchi S, Kimura J, Yonekura Y, et al. Altered cerebral energy metabolism in Alzheimer's disease: a PET study. J Nucl Med 1994;35:1–6.
13. Minoshima S, Foster NL, Kuhl DE. Posterior cingulate cortex in Alzheimer's disease. Lancet 1994;344:895.
14. Minoshima S, Giordani B, Berent S, Frey KA, Foster NL, Kuhl DE. Metabolic reduction in the posterior cingulate cortex in very early Alzheimer's disease. Ann Neurol 1997;42:85–94.
15. Bartlett EJ, Brodie JD, Wolf AP, Christman DR, Laska E, Meissner M. Reproducibility of cerebral glucose metabolic measurements in resting human subjects. J Cereb Blood Flow Metab 1988;8:502–12.
16. Maquet P, Dive D, Salmon E, von Frenckel R, Franck G. Reproducibility of cerebral glucose utilization measured by PET and the [^{18}F]-2-fluoro-2-deoxy-D-glucose method in resting, healthy human subjects. Eur J Nucl Med 1990;16:267–73.
17. Wang GJ, Volkow ND, Overall J, Hitzemann RJ, Pappas N, Pascani K, et al. Reproducibility of regional brain metabolic responses to lorazepam. J Nucl Med 1996;37:1609–13.
18. Tyler JL, Strother SC, Zatorre RJ, Alivisatos B, Worsley KJ, Diksic M, et al. Stability of regional cerebral glucose metabolism in the normal brain measured by positron emission tomography. J Nucl Med 1988;29:631–42.
19. Phelps ME, Huang SC, Hoffman EJ, Selin C, Sokoloff L, Kuhl DE. Tomographic measurement of local cerebral glucose metabolic rate in humans with (F-18)2-fluoro-2-deoxy-D-glucose: validation of method. Ann Neurol 1979;6:371–88.

20. Reivich M, Alavi A, Wolf A, Fowler J, Russell J, Arnett C, et al. Glucose metabolic rate kinetic model parameter determination in humans: the lumped constants and rate constants for [^{18}F]fluorodeoxyglucose and [^{11}C]deoxyglucose. J Cereb Blood Flow Metab 1985;5:179–92.
21. Tataranni PA, Gautier JF, Chen K, Uecker A, Bandy D, Salbe AD, et al. Neuroanatomical correlates of hunger and satiation in humans using positron emission tomography. Proc Natl Acad Sci USA 1999;96:4569–74.
22. Routh VH. Glucose-sensing neurons: are they physiologically relevant? Physiol Behav 2002;76:403–13.
23. Pardridge WM, Boado RJ, Farrell CR. Brain-type glucose transporter (GLUT-1) is selectively localized to the blood–brain barrier: studies with quantitative western blotting and in situ hybridization. J Biol Chem 1990;265:18035–40.
24. Maher F, Vannucci SJ, Simpson IA. Glucose transporter proteins in brain. FASEB J 1994;8:1003–11.
25. Nagamatsu S, Sawa H, Kamada K, Nakamichi Y, Yoshimoto K, Hoshino T. Neuron-specific glucose transporter (NSGT): CNS distribution of GLUT3 rat glucose transporter (RGT3) in rat central neurons. FEBS Lett 1993;334:289–95.
26. Asano T, Katagiri H, Takata K, Tsukuda K, Lin JL, Ishihara H, et al. Characterization of GLUT3 protein expressed in Chinese hamster ovary cells. Biochem J 1992;288:189–93.
27. Yano H, Seino Y, Inagaki N, Hinokio Y, Yamamoto T, Yasuda K, et al. Tissue distribution and species difference of the brain type glucose transporter (GLUT3). Biochem Biophys Res Commun 1991;174:470–7.
28. Ito H. The summary of "Treatment guidelines of diabetes mellitus in the elderly people" drafted by a group of comprehensive research on aging and health (in Japanese). Geriatric Med 1996;34:899–902.

序にかえて

谷内一彦*1　須原哲也*2

■ はじめに

分子イメージング法とは，生体内のタンパク量や酵素活性，遺伝子の発現レベルなどをin vivoで可視化する技術であり，病態解明や臨床検査，薬効評価など様々な分野に応用されている。ヒト個体レベルでの評価においては，生体内分子に特異的に結合する化合物（プローブ）をポジトロン放出核種で標識し，ポジトロン断層撮影法（PET）でその空間分布を体外計測するのが代表的な手法である。PETは三次元画像情報を定量的かつ高感度に入手できることが利点であり，生体組織内のフェムトモル濃度のプローブの体外からの検出を可能とする。PETは消滅γ線を用いて正確な微量三次元情報を得ることからART（Annihilation Radiation Tomography）とも言われている。さらに小動物と同じプローブで臨床試験を実施することが可能であることも利点である。最近では，アルツハイマー病などの神経疾患の脳内に特異的に蓄積する異常タンパクの定量化[1]や遺伝子発現量の解析による遺伝子治療の効果判定などにも活用されつつある。また新規化合物のヒト体内における挙動をin vivoで評価できることから，早期医薬品開発スクリーニングにおける新たなツールとして，創薬分野への導入も進んでいる[2]。最近の技術革新をコストと時間のかかる創薬に利用して効率化を図ることが期待され，実際に国際学会に参加するとビッグ・ファーマからの分子イメージングを用いた演題に遭遇し，特に創薬における早期スクリーニング，統合失調症[3]やアルツハイマー病，癌[4]への応用で注目を集めている。個体レベルでのイメージング研究はこれまで核医学がカバーしてきた領域であるが，最近の基盤技術の進歩により核医学の領域を超えて医学，薬学，工学の新しい融合領域として期待されている。図1に我々の考える分子イメージングの理想像を示す。

❶ 新規プローブの臨床応用：臨床研究と治験

PETプローブによる臨床研究を開始するに当たっては，一般臨床医薬品とは異なった特殊性がある。その特殊性とは核医学的手法に関係する以下のような点である：通常の投与量は1μg以下で極めて微量である，多くは単回静脈内投与であり，反復して投与されることは少ない。このような特徴から，新規PETプローブを臨床使用するに当たっては，その安全性評価は一般医薬品よりも緩和した条件でよいという考え方が欧米を中心に一般化しつつある。投与量や安全性に関する国際基準は今のところ存在しないが，European Medicines Agency（EMEA）のポジションペーパーでは，有効量の100分の1未満で，100μg以下の用量であればヒトに投与してもよ

*1 K. Yanai　東北大学大学院医学系研究科　機能薬理学分野　*2 T. Suhara　放射線医学総合研究所　分子イメージング研究センター　分子神経イメージング研究グループ
〔索引用語：PET，脳機能，分子イメージング，創薬，マイクロドージング〕